Materials Horizons

2D PtS nanorectangles/g-C3N4 nanosheets with metal sulfide-support interaction effect for high-efficiency photocatalytic H2 evolution

Journal:	*Materials Horizons*
Manuscript ID	MH-COM-10-2020-001693.R1
Article Type:	Communication
Date Submitted by the Author:	20-Nov-2020
Complete List of Authors:	Lin, Bo; University of Electronic Science and Technology of China, Zhou, Yao; Nanyang Technological University Xu, Baorong; Xi'an Jiaotong University Zhu, Chao; Nanyang Technological University Tang, Wu; University of Electronic Science and Technology of China, State Key Laboratory of Electronic Thin Films and Integrated Devices Niu, Yingchun; China University of Petroleum Beijing Di, Jun; Nanyang Technological University Song, Pin ; Nanyang Technological University, School of Materials Science and Engineering Zhou, Jiadong ; Nanyang Technological Univeristy, School of Materials Science and Engineering Luo, Xiao; University of Electronic Science and Technology of China Kang, Lixing; Nanyang Technological University Duan, Ruihuan; Nanyang Technological University Fu, Qundong; Nanyang Technological University, School of Materials Science and Engineering Liu, Haishi ; University of Electronic Science and Technology of China Jin, Ronghua; Xi'an Jiao Tong University,, Xue, Chao; Zhengzhou University, School of Materials Science and Engineering Chen, QIang; Sun Yat-Sen University, School of Chemical Engineering and Technology Yang, Guidong; School of Energy & Power Engineering, Xi'an Jiaotong University, Varga, Kalman ; Vanderbilt University, Physics and Astronomy Xu, Quan; China University of Petroleum (Beijing), Institute of New Energy Li, Yonghui; Tianjin University Liu, Zheng; Nanyang Technological University, School of Mechanical Engineering and Materials Science Liu, Fucai; University of Electronic Science and Technology of China,

A table of contents entry

2D PtS nanorectangles/g-C_3N_4 nanosheets with metal sulfide-support interaction effect achieve an ultrahigh photocatalytic H_2 evolution rate.

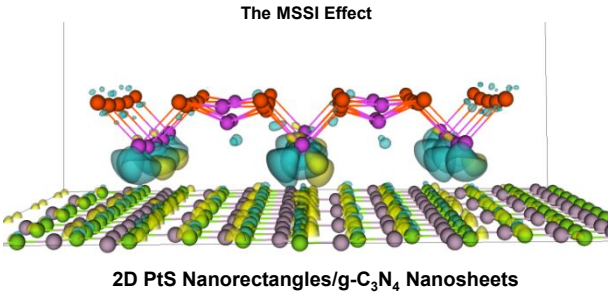

COMMUNICATION

2D PtS nanorectangles/g-C_3N_4 nanosheets with metal sulfide-support interaction effect for high-efficiency photocatalytic H_2 evolution

Received 00th January 20xx,
Accepted 00th January 20xx

DOI: 10.1039/x0xx00000x

Bo Lin,[+a] Yao Zhou,[+b] Baorong Xu,[c] Chao Zhu,[d] Wu Tang,[e] Yingchun Niu,[f] Jun Di,[d] Pin Song,[d] Jiadong Zhou,[d] Xiao Luo,[a] Lixing Kang,[d] Ruihuan Duan,[d] Qundong Fu,[d] Haishi Liu,[a] Ronghua Jin,[c] Chao Xue,[g] Qiang Chen,[h] Guidong Yang,[c] Kalman Varga,[i] Quan Xu,*[f] Yonghui Li,*[j] Zheng Liu*[d] and Fucai Liu*[a]

The cocatalyst design is a key approach to acquire high solar-energy conversion efficiency for photocatalytic hydrogen evolution. Here a new in-situ vapor-phase (ISVP) growth method is developed to construct the cocatalyst of 2D PtS nanorectangles (a length of ~7 nm, a width of ~5 nm) on the surface of g-C_3N_4 nanosheets. The 2D PtS nanorectangles/g-C_3N_4 nanosheets (PtS/CN) shows an unusual metal sulfide-support interaction (MSSI), which is evidenced by atomic resolution HAADF-STEM, synchrotron-based GIXRD, XPS and DFT calculations. The effect of MSSI contributes to the optimization of geometrical structure and energy-band structure, acceleration of charge transfer, and reduction of hydrogen adsorption free energy of PtS/CN, thus yielding excellent stability and ultrahigh photocatalytic H_2 evolution rate of 1072.6 μmol h^{-1} (an apparent quantum efficiency of 45.7% at 420 nm), up to 13.3 and 1532.3 times by contrast with that of Pt nanoparticles/g-C_3N_4 nanosheets and g-C_3N_4 nanosheet, respectively. This work would provide a new platform for designing high-efficiency photocatalysts for sunlight-driven hydrogen generation.

[a] *School of Optoelectronic Science and Engineering, University of Electronic Science and Technology of China, Chengdu 611731, China. E-mail: fucailiu@uestc.edu.cn*
[b] *School of Physical and Mathematical Sciences, Nanyang Technological University, Singapore 637371, Singapore*
[c] *XJTU-Oxford International Joint Laboratory for Catalysis, School of Chemical Engineering and Technology, Xi'an Jiaotong University, Xi'an 710049, China*
[d] *School of Materials Science and Engineering, Nanyang Technological University, Singapore 639798, Singapore. E-mail: z.liu@ntu.edu.sg*
[e] *School of Materials and Energy, University of Electronic Science and Technology of China, Chengdu 611731, China*
[f] *State Key Laboratory of Heavy Oil Processing, China University of Petroleum-Beijing, Beijing 102249, China. Email: xuquan@cup.edu.cn*
[g] *State Centre for International Cooperation on Designer Low-carbon and Environmental Materials (CDLCEM), School of Materials Science and Engineering, Zhengzhou University, Zhengzhou 450001, China*
[h] *School of Chemical Engineering and Technology, Sun Yat-sen University (Zhuhai Campus), Zhuhai 519082, China*
[i] *Department of Physics and Astronomy, Vanderbilt University, Nashville, Tennessee 37235, USA*
[j] *Department of Physics and Tianjin Key Laboratory of Low Dimensional Materials Physics and Preparing Technology, School of Science, Tianjin University, Tianjin 300350, China. Email: yonghui.li@tju.edu.cn*
[+] *Bo Lin and Yao Zhou contributed equally to this work.*

New concepts

In this article, the concept of metal sulfide-support interaction (MSSI) has been demonstrated to reveal the interaction between the metal ingredient of 2D transition metal chalcogenides (TMCs) and supports under high-temperature H_2 reduction. This study is of great importance to the development of the classical research of strong metal support interaction (SMSI), which is a famous theory in the fields of materials science, energy, and catalysis. This study covers the complete research trajectory from the generation of MSSI to its application in photocatalytic H_2 evolution. More importantly, the MSSI has an effect on the geometrical structure, electronic band structure, and charge transfer of TMCs/supports, thus boosting the activity of photocatalytic H_2 evolution significantly. This work opens a new opportunity for the design of advanced heterostructured nanomaterials with high catalytic activity.

Introduction

Sunlight-driven water splitting for hydrogen production over semiconductor photocatalysts is a promising and green route to advance solar-energy conversion into fuels.[1, 2] The efficiency of photocatalytic conversion has long relied on suppressing the recombination of electron-hole pairs and boosting surface redox reaction.[3, 4] The use of cocatalysts reduces the overpotential or activation energy of hydrogen evolution reaction, accelerates the separation and transfer of charges, and provides plentiful adsorption and reaction active sites for H_2O molecules, which are beneficial to the enhancement of overall photocatalytic conversion efficiency.[5-8] Among diverse cocatalysts, Pt has been regarded to be the most commonly used cocatalyst with the high activity for photocatalytic H_2 evolution.[9-11] However, the scarcity and high material cost of Pt cocatalyst limit its actual applications. Therefore, from the perspective of cocatalyst design, development of novel cocatalysts with higher performance and lower cost than Pt is urgently needed.

Recently, as a new member of transition metal chalcogenides, PtS has triggered keen interests due to its excellent mechanical performance, outstanding electronic, and optical properties.[12-14] More importantly, PtS has a typical 2D layered architecture with

massive exposed surfaces and highly active basal-plane sites, which enable it to be an ideal candidate as the cocatalyst for photocatalytic H_2 evolution.[15, 16] Moreover, in the design of cocatalysts, reducing the size of 2D layered cocatalysts to the nano-level (less than 10 nm) can endow them with multiple fascinating properties, such as excellent light harvesting capability, high surface-to-volume ratio, massive electron accumulation sites, more exposed active surface and edges, which are highly conducive to the visible-light-driven H_2 generation.[17-21] Therefore, based on the consideration of cocatalyst design presented above, constructing 2D nano-level PtS sheets on semiconductor photocatalysts would provide an attractive approach to acquire the photocatalytic system with high solar-energy conversion efficiency. Unfortunately, attempts to achieve 2D PtS-based heterojunctions with high photocatalytic activity have still met extremely limited success.

Here we develop a new in-situ vapor-phase (ISVP) growth method to synthesize novel 2D PtS nanorectangles/g-C_3N_4 nanosheets (PtS/CN) with an unusual metal sulfide-support interaction (MSSI), where 2D rectangle-like PtS nanosheets (a length of ~7 nm, a width of ~5 nm) grow on the surface of g-C_3N_4 nanosheet. The effect of MSSI contributes to significantly enhanced visible-light harvesting, fast charge transfer, and decreased hydrogen adsorption free energy, which cooperatively lead to an ultrahigh photocatalytic H_2 evolution activity of 1072.6 μmol h^{-1} (an apparent quantum efficiency of 45.7% at 420 nm), up to 13.3 and 1532.3 times by contrast with that of g-C_3N_4 nanosheet loaded with the same amount of Pt and g-C_3N_4 nanosheet, respectively.

Results and Discussion

Synthesis and morphological property

The formation of 2D PtS nanorectangles/g-C_3N_4 nanosheets is relying on a novel in-situ vapor-phase (ISVP) growth method. As shown in Fig. 1a, bulk g-C_3N_4 was synthesized via the thermal-induced self-condensation of melamine in a mixed atmosphere (20% H_2 + 80% Ar) as reported previously,[22] and g-C_3N_4 nanosheet (CN) was synthesized via the thermal exfoliation of bulk g-C_3N_4 annealing in air atmosphere. Then synthetic CN was dispersed in an aqueous solution containing H_2PtCl_6, where the generated $[PtCl_6]^{2-}$ group absorbed on the surface of g-C_3N_4 to obtain the $[PtCl_6]^{2-}$/CN. Subsequently, the above $[PtCl_6]^{2-}$/CN and sulfur powder were synchronously heated to 550 °C in H_2

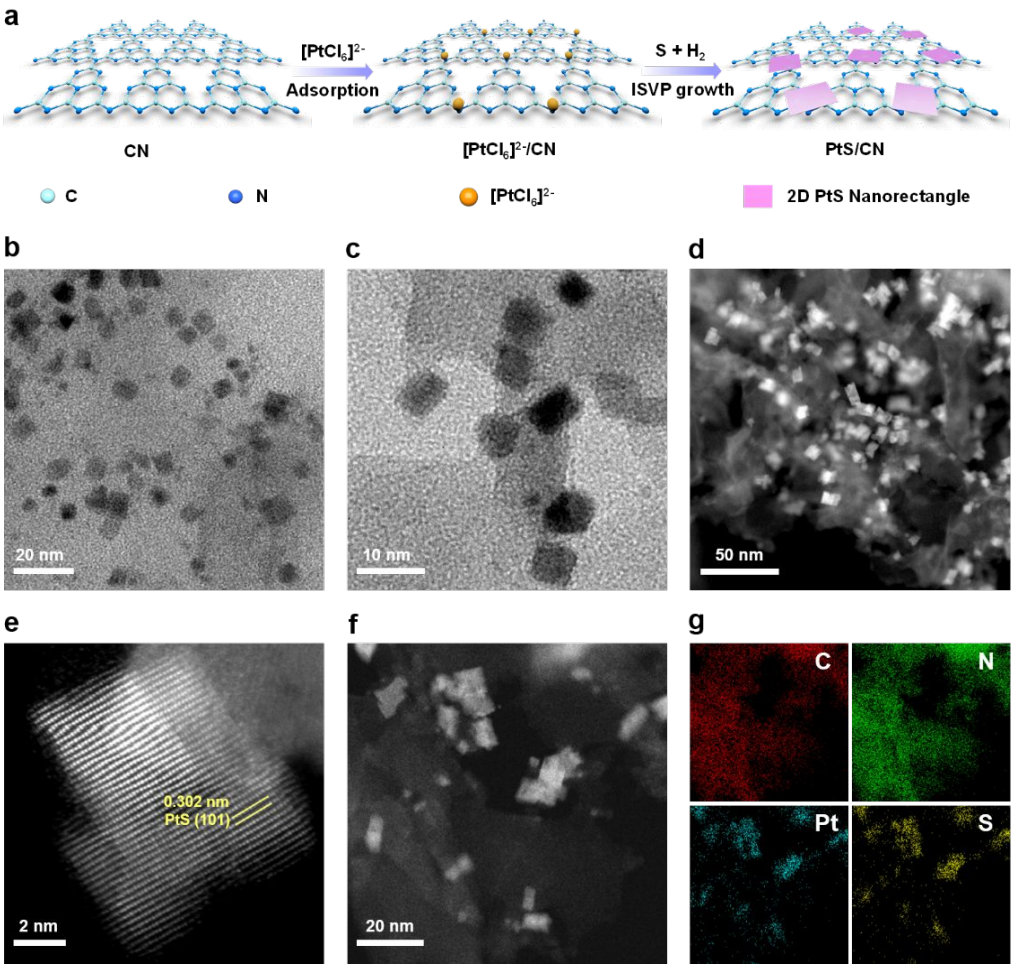

Fig. 1 Synthesis and Surface morphology of PtS/CN. (a) Schematic of the synthesis of PtS/CN using a new in-situ vapor-phase (ISVP) growth method. (b,c) TEM images of PtS/CN. (d) HAADF-STEM image of PtS/CN. (e) Atom-resolved HAADF-STEM image of PtS/CN. (f) HAADF-STEM image and (g) corresponding mapping images of C, N, Pt and S.

COMMUNICATION

atmosphere. Under high temperature, the formed H_2S through the interaction of S and H_2 can reduce the $[PtCl_6]^{2-}$ group to generate PtS seed crystals, which grew on the surface of g-C_3N_4 support to generate the MSSI. Notably, owning to the MSSI effect, PtS seed crystals tend to grow into 2D nano-sized rectangle-like sheets to obtain PtS/CN.[23] The presence of MSSI can be well evidenced by transmission electron microscopy (TEM) and high-angle annular dark-field scanning transmission electron microscopy (HAADF-STEM) images of PtS/CN. Fig. 1b-d show that PtS nanorectangles have a typical 2D rectangle-like sheet structure with a length of ~7 nm and a width of ~5 nm due to the MSSI effect, and they are anchored uniformly on the surface of g-C_3N_4 nanosheet to form the binary metal sulfide-support photocatalyst. To disclose the fine structure of PtS/CN, atomic-resolution HAADF-STEM is performed. As shown in Fig. 1e and Fig. S1 (ESI), the lattice-fringe spacing of 0.302 nm belongs to the (101) reflection plane of tetragonal PtS, and this (101) plane grew on the amorphous region of g-C_3N_4 support, indicating the successful construction of metal sulfide-support system. Elemental mappings (Fig. 1f,g) and EDX image (Fig. S2, ESI) further support the presence of 2D PtS nanorectangles/g-C_3N_4 nanosheets.

Crystallography and chemical compositions

X-ray diffraction patterns (XRD, Fig. 2a) show that CN displays two XRD peaks of 13.1° and 27.7°, corresponding to (100) and (002) crystal planes of g-C_3N_4, respectively.[24, 25] For PtS/CN, the (002) reflection peak of g-C_3N_4 shifts from 27.7° to 27.9°, which is probably due to the effect of MSSI through chemical coupling with PtS, and all other XRD peaks are attributed to the crystal planes of tetragonal PtS (JCPDS #18-0972). To further illuminate the MSSI effect on the crystallinity and crystallographic orientation of 2D PtS nanorectangles in PtS/CN, the synchrotron-based grazing-incidence X-ray diffraction (2D-GIXRD) was performed. As shown in Fig. 2b,c, the scattered rings at q of 11.3, 19.3 and 14.7 nm^{-1} correspond to the (100) and (002) diffraction of g-C_3N_4 as well as the (101) diffraction of PtS, respectively, indicating the preferred crystallographic orientation of (101) crystal plane of PtS on the support of g-C_3N_4 due to the MSSI effect. Additionally, the surface chemical state of PtS/CN was investigated by X-ray photoelectron spectroscopy (XPS). The signals in C 1s region (Fig. 2d and Fig. S3a, ESI) indicate the presence of C─C (284.8 eV) and N─C═N (286.4 and 288.3 eV) in melon networks of g-C_3N_4, respectively.[26, 27] In N 1s region (Fig. 2e), the peaks at 398.7 and 400.3 eV were due to the C─N═C and N─$(C)_3$ groups, respectively, which show a shift toward the higher binding energy by 0.20 eV compared to that of g-C_3N_4 (Fig. S3b, ESI), besides, the peaks at 403.0 and 404.5 eV are attributed to the charging effect in the heterocycles of g-C_3N_4.[22, 27] Moreover, the peak at 401.1 eV for N-H disappears in Fig. 2e compared to that of g-C_3N_4 (Fig. S3b, ESI) possibly due to the effect of PtS. As shown in Fig. 2f and Fig. S4 (ESI), the two peaks in S 2p region at 162.7 and 163.9 eV correspond to S $2p_{3/2}$ and S $2p_{1/2}$ in PtS, respectively, while the two peaks in Pt 4f region at 71.7 and 75.3 eV correspond to Pt $4f_{7/2}$ and Pt $4f_{5/2}$, respectively.[13] Of note, the Pt peak at 71.7 eV displays a shift toward the lower binding energy in comparison with that of PtS in Fig. S4b (ESI). Hence, in consideration of the shifts to higher B.E. for the peaks of N 1s (398.7 and 400.3 eV) and lower B.E. for the peak of Pt 4f (71.7 eV) in PtS/CN, the XPS results indicate the presence of metal sulfide-support interaction between g-C_3N_4 support and PtS, suggesting the electron transfer from g-C_3N_4 to PtS.[1, 2, 28]

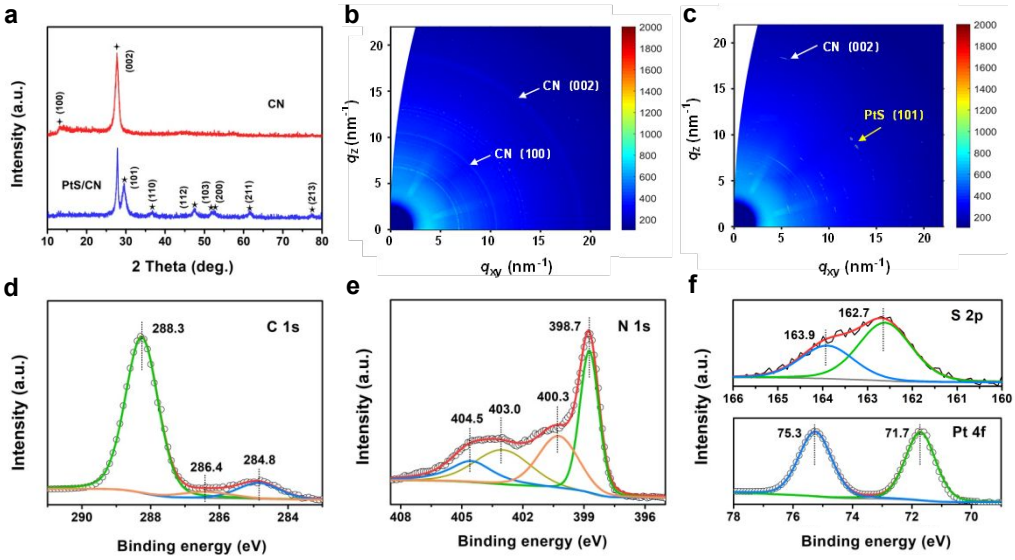

Fig. 2 Crystallography and Chemical structure. a) XRD patterns of CN and PtS/CN. Synchrotron-based 2D-GIXRD profiles of b) CN and c) PtS/CN. XPS spectra of PtS/CN in the regions of d) C 1s, e) N 1s, f) S 2p and Pt 4f.

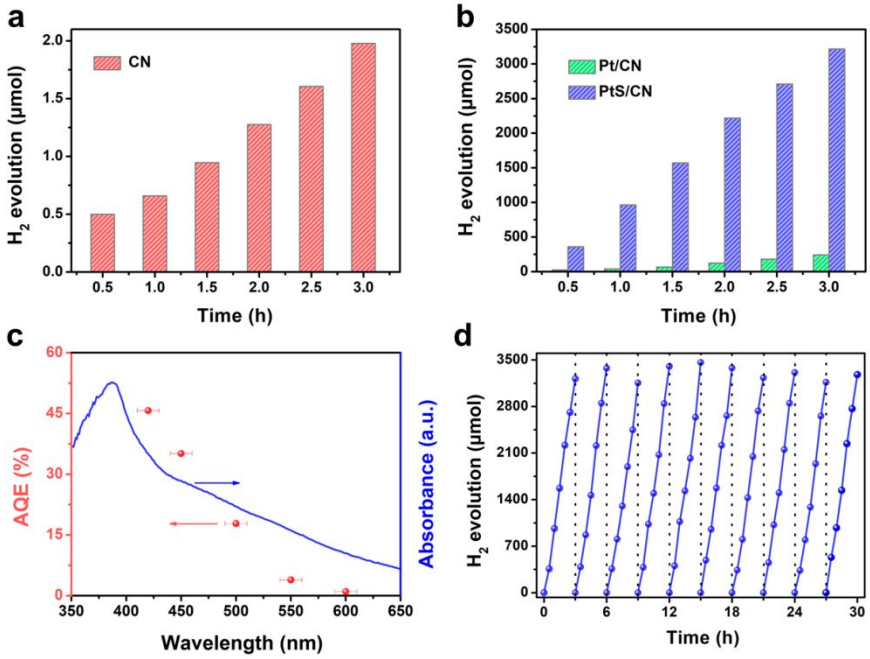

Fig. 3 Photocatalytic H_2 evolution activity tests. Time-dependent photocatalytic H_2 evolution of a) CN, b) Pt/CN and PtS/CN under visible-light irradiation (λ>420 nm). c) Wavelength-dependent AQE for photocatalytic H_2 evolution over PtS/CN. d) Cycling tests of photocatalytic H_2 evolution over PtS/CN.

Photocatalytic H_2 evolution performance

Time-dependent photocatalytic H_2 evolution of different samples was performed with triethanolamine as the hole scavenger under visible-light irradiation (λ>420 nm). As shown in Fig. 3a, CN shows a negligible photocatalytic hydrogen-evolution rate (HER) of 0.7 μmol h^{-1} due to its inferior charge-transfer capacity. Incredibly, PtS/CN with the optimal cocatalyst-loading amount shows an ultrahigh HER of 1072.6 μmol h^{-1} (Fig. 3b and Fig. S5, ESI), up to 13.3 and 1532.3 times and by contrast with that of g-C_3N_4 nanosheet loaded with the same amount of Pt (Pt/CN, 80.9 μmol h^{-1}) and CN, respectively, strongly evidencing the advantages of MSSI effect. The apparent quantum efficiency (AQE) of PtS/CN was estimated to be 45.7% at 420 ± 10 nm, far outperforming the majority of g-C_3N_4-based photocatalysts with Pt as the cocatalyst in previous reports (Fig. 3c and Table S1, ESI).[25, 29-35] The stability and recyclability of H_2 evolution for PtS/CN was investigated. As shown in Fig. 3d, PtS/CN remains largely unchanged photocatalytic activity for H_2 evolution after 10 consecutive cycling tests, indicating excellent stability, as evidenced by the similar XRD patterns of fresh PtS/CN and recycled PtS/CN as well as the TEM image of recycled PtS/CN (Fig. S6 and Fig. S7, ESI). The ultrahigh photocatalytic activity and excellent stability of PtS/CN well evidence the presence of the MSSI effect.

Optical and photoelectric properties

It has been well proved that the MSSI effect contributes to the formation of 2D nanorectangle structure of PtS and ultrahigh photocatalytic H_2 evolution rate of PtS/CN. To further shed light on the intrinsic relationship between MSSI and photocatalytic activity, optical and photoelectric properties of PtS/CN were investigated. In the UV-vis diffuse reflectance spectra (DRS) of CN and PtS/CN (Fig. 4a), PtS/CN displays a much stronger optical absorption ability than CN in the ultraviolet and visible-light region due to the presence of 2D PtS cocatalyst and the effect of MSSI.[36] The photoinduced charge separation and transfer property of synthetic samples was studied by a variety of characterizations of spectra. The transient photocurrent responses (Fig. 4b) show that PtS/CN displays a far higher photocurrent density of 3.39 μA cm^{-2}, up to 2.9 times by contrast with that of CN, indicative of a significantly enhanced charge separation and transfer efficiency.[37, 38] Photoluminescence (PL) spectra (Fig. 4c) and electrochemical impedance spectroscopy (Fig. 4d) support the above result, where PtS/CN displays a much lower emission peak intensity and the smaller radius of Nyquist circle by contrast with CN, revealing the advantages of MSSI on accelerating the migration of photoinduced charges.[39-42]

Theoretical study

To further explore the action mechanism of MSSI nature on photocatalytic H_2 generation activity, density functional theory (DFT) calculations were carried out (Fig. 5). As illustrated in Fig. S8, Fig. S9 and Fig. S10 (ESI), the MSSI between PtS and g-C_3N_4 can be constructed in the PtS/CN system, well supporting the HAADF-STEM, 2D-GIXRD and XPS results of the presence of MSSI. Furthermore, with the assistance of MSSI, the formed Pt-Pt-Pt bonds on the (001) and (010) directions in the structure of PtS can offer the surface constrained force to lead to the generation of 2D nanorectangle structure of PtS (Fig. 5a). The density of states (DOS) of CN, PtS nanorectangle and PtS/CN was calculated. Through the comparison of DOS trend between PtS nanorectangle (Fig. 5b) and bulk PtS (Fig. S11, ESI), it can be found that the band gap of PtS nanorectangle is closed by the surface states of Pt-Pt-Pt bonds. Such a character shown in nano-scale PtS and PtS/CN explains the enhancement of visible-light

absorption, which is a result of the MSSI effect. Moreover, as shown in Fig. 5c and Fig. S12 (ESI), the surface of PtS can extract electron density from adjacent g-C_3N_4 in PtS/CN system, indicative of the acceleration of charge separation and transfer induced by MSSI,[43, 44] consistent with the results of photocurrent response and PL. Additionally, the Gibbs free energy (ΔG_{H^*}) was calculated to evaluate hydrogen adsorption and reaction energy barrier of photocatalytic H_2 evolution. As displayed in Fig. 5d, PtS/CN exhibits a far smaller negative value of ΔG_{H^*} (-0.07 eV) than that of previously reported g-C_3N_4 (-0.58 eV) and Pt/g-C_3N_4 (-0.29 eV),[45, 46] strongly manifesting that the MSSI effect existed in PtS/CN is kinetically favorable for the reduction of free energy barrier to accelerate H_2 evolution.[47-49]

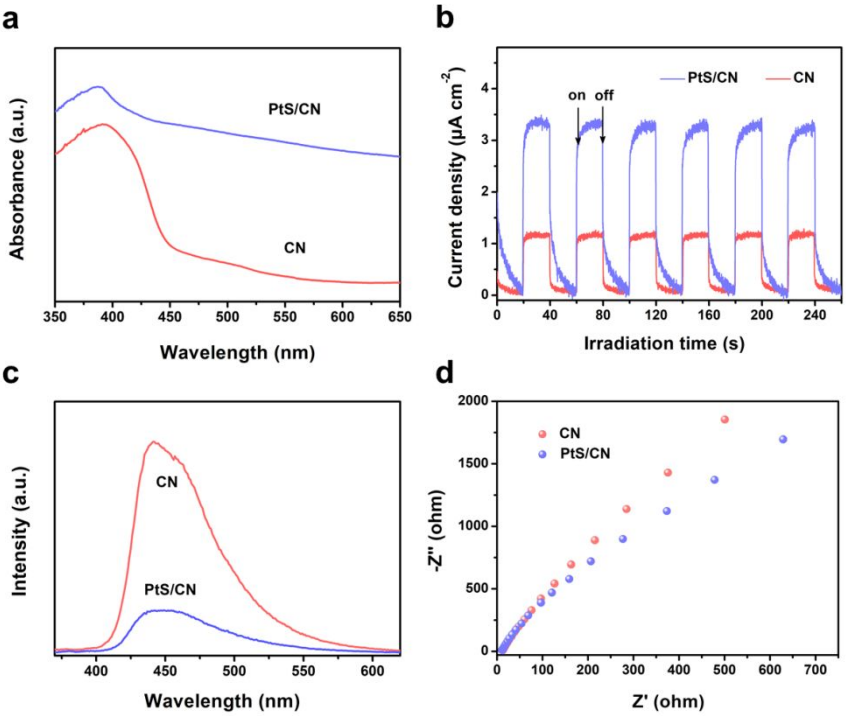

Fig. 4 Optical and photoelectric property. a) UV-vis diffuse reflectance spectra of CN and PtS/CN. b) Transient photocurrent responses of CN and PtS/CN. c) Photoluminescence spectra of CN and PtS/CN. d) EIS Nyquist plots of CN and PtS/CN.

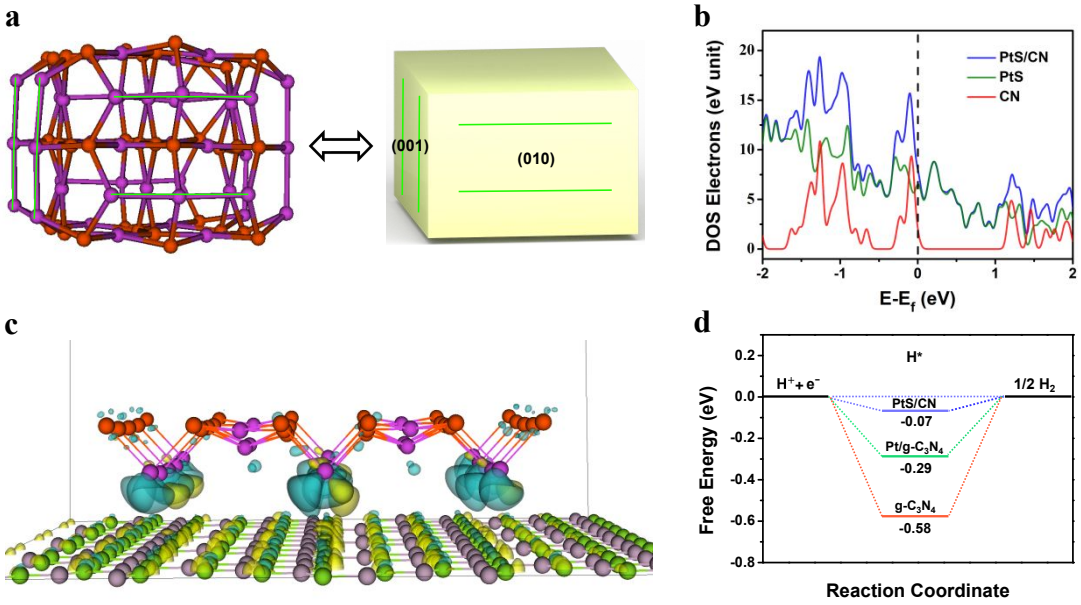

Fig. 5 Theoretical study. a) The geometrical structure of 2D PtS nanorectangles optimized using DFT. Purple and orange spheres represent Pt and S atoms, respectively. Fluorescent-green strip represents the Pt-Pt-Pt bond. b) Calculated energy band structure of CN, PtS nanorectangle and PtS/CN. c) The side view of charge density difference for PtS/CN. Blue and yellow regions represent the electron accumulation and depletion, respectively. d) The free energy diagram of hydrogen evolution for g-C_3N_4, Pt/g-C_3N_4 and PtS/CN.

According to all results presented above, an underlying mechanism for photocatalytic H_2 evolution has been proposed. Under visible-light irradiation (λ>420 nm), g-C_3N_4 nanosheets can be excited to generate photoexcited electrons and holes. The photoexcited holes are consumed by the scavenger of triethanolamine, while the photoexcited electrons transfer to 2D PtS nanorectangles to reduce the H^+ in aqueous solution to generate H_2. It is worth mentioning that the unique MSSI in 2D PtS nanorectangles/g-C_3N_4 nanosheets is responsible for ultrahigh photocatalytic activity and excellent stability of PtS/CN. Firstly, the MSSI has a strong impact on the formation of 2D PtS nanorectangles. Such 2D PtS nanorectangles can provide more active sites than Pt nanoparticles with the same amount of Pt for g-C_3N_4 in photocatalytic H_2 evolution, although loading 2D PtS nanorectangles may block some pores existed in the g-C_3N_4 nanosheets (Fig. S13 and Table S2, ESI). Secondly, the MSSI is beneficial to the potential optimization of electronic structure of supported PtS, thus facilitating optical absorption and excitation of photoinduced charges for PtS/CN (Fig. 4a and Fig. 5b). Additionally, the MSSI can significantly accelerate charge transfer from g-C_3N_4 to PtS (Fig. 4b-d, Fig. 5c and Fig. S12, ESI). Lastly, the MSSI can decrease the hydrogen adsorption free energy to speed up the kinetical process of photocatalytic H_2 generation reaction as well (Fig. 5d).

CONCLUSIONS

In summary, 2D PtS nanorectangles/g-C_3N_4 nanosheets have been successfully synthesized using a novel in-situ vapor-phase growth method. Through the experimental and calculated results, we have revealed an unusual metal sulfide-support interaction effect (MSSI) between PtS and g-C_3N_4. The MSSI can efficiently prompt PtS/CN to realize the optimization of geometrical structure, the acceleration of excitation, the separation and transfer of photoinduced charges as well as the reduction of hydrogen adsorption free energy, thus contributing to a ultrahigh photocatalytic H_2 evolution activity of 1072.6 μmol h^{-1} (an AQE of 45.7% at 420 nm) for PtS/CN, up to 13.3 and 1532.3 times by contrast with that of Pt/CN and CN, respectively.

Conflicts of interest

There are no conflicts to declare.

Acknowledgements

This work was funded by the China Postdoctoral Science Foundation (pre-station, Grant No. 2019TQ0050), Applied Basic Research Program of Sichuan Province (Grant No. 2020YJ0068), the China Postdoctoral Science Foundation (Grant No. 2020M673186), National Natural Science Foundation of China (Grant No. 22002014), National Natural Science Foundation of China (Grant No. 11804248), Natural Science Foundation of Tianjin (Grant No. 18JCQNJC03200), and Sichuan Province Key Laboratory of Display Science and Technology. This work is also supported by MOE Tier 1 RG4/17 and MOE Tier 2 MOE2019-T2-2-105. This work used the Extreme Science and Engineering Discovery Environment (XSEDE), which is supported by the National Science Foundation (ACI-1548562). K.V. was supported by the NSF under Grant No. IRES 1826917.

References

1 V. W. Lau, I. Moudrakovski, T. Botari, S. Weinberger, M. B. Mesch, V. Duppel, J. Senker, V. Blum and B. V. Lotsch, *Nat. Commun.*, 2016, **7**, 12165.

2 V. W. Lau, V. W. Yu, F. Ehrat, T. Botari, I. Moudrakovski, T. Simon, V. Duppel, E. Medina, J. K. Stolarczyk, J. Feldmann, V. Blum and B. V. Lotsch, *Adv. Energy Mater.,* 2017, **7**, 1602251.

3 W. Bi, X. Li, L. Zhang, T. Jin, L. Zhang, Q. Zhang, Y. Luo, C. Wu and Y. Xie, *Nat. Commun.,* 2015, **6**, 8647.

4 Z. Lian, M. Sakamoto, Y. Kobayashi, N. Tamai, J. Ma, T. Sakurai, S. Seki, T. Nakagawa, M. W. Lai and M. Haruta, *ACS Nano,* 2019, **13**, 8356-8363.

5 K. Khan, X. Tao, M. Shi, B. Zeng, Z. Feng and C. Li, *Adv. Funct. Mater.,* 2020, **30**, 2003731.

6 D. Zheng, X. N. Cao and X. Wang, *Angew. Chem. Int. Ed.,* 2016, **55**, 11512-11516.

7 S. Hejazi, S. Mohajernia, B. Osuagwu, G. Zoppellaro, P. Andryskova, O. Tomanec, S. Kment, R. Zboril and P. Schmuki, *Adv. Mater.*, 2020, **32**, 1908505.

8 B. Lin, Z. Chen, P. Song, H. Liu, L. Kang, J. Di, X. Luo, L. Chen, C. Xue, B. Ma, G. Yang, J. Tang, J. Zhou, Z. Liu and F. Liu, *Small*, 2020, **16**, 2003302.

9 H. Zhang, P. Zhang, M. Qiu, J. Dong, Y. Zhang and X. W. Lou, *Adv. Mater.*, 2019, **31**, 1804883.

10 S. Bai, L. Yang, C. Wang, Y. Lin, J. Lu, J. Jiang and Y. Xiong, *Angew. Chem. Int. Ed.*, 2015, **54**, 14810-14814.

11 Z. Liang, R. Shen, Y. H. Ng, P. Zhang, Q. Xiang and X. Li, *J. Mater. Sci. Technol.*, 2020, **56**, 89-121.

12 J. Yu, S. Seo, Y. Luo, Y. Sun, S. Oh, C. T. K. Nguyen, C. Seo, J. H. Kim, J. Kim and H. Lee, *ACS Nano*, 2020, **14**, 1715-1726.

13 J. Huang, N. Dong, N. McEvoy, L. Wang, C. O. Coileain, H. Wang, C. P. Cullen, C. Chen, S. Zhang, L. Zhang and J. Wang, *ACS Nano*, 2019, **13**, 13390-13402.

14 J. McAllister, N. A. G. Bandeira, J. C. McGlynn, A. Y. Ganin, Y. Song, C. Bo and H. N. Miras, *Nat. Commun.*, 2019, **10**, 370.

15 J. Zhou, J. Lin, X. Huang, Y. Zhou, Y. Chen, J. Xia, H. Wang, Y. Xie, H. Yu, J. Lei, D. Wu, F. Liu, Q. Fu, Q. Zeng, C. H. Hsu, C. Yang, L. Lu, T. Yu, Z. Shen, H. Lin, B. I. Yakobson, Q. Liu, K. Suenaga, G. Liu and Z. Liu, *Nature*, 2018, **556**, 355-359.

16 J. Zhou, X. Kong, M. C. Sekhar, J. Lin, F. L. Goualher, R. Xu, X. Wang, Y. Chen, Y. Zhou, C. Zhu, W. Lu, F. Liu, B. Tang, Z. Guo, C. Zhu, Z. Cheng, T. Yu, K. Suenaga, D. Sun, W. Ji and Z. Liu, *ACS Nano*, 2019, **13**, 10929-10938.

17 Y. Liu, H. Zhang, J. Ke, J. Zhang, W. Tian, X. Xu, X. Duan, H. Sun, M. O. Tade and S. Wang, *Appl. Catal. B: Environ.*, 2018, **228**, 64-74.

18 X. Y. Liu, H. Chen, R. Wang, Y. Shang, Q. Zhang, W. Li, G. Zhang, J. Su, C. T. Dinh, F. P. G. D. Arquer, J. Li, J. Jiang, Q. Mi, R. Si, X. Li, Y. Sun, Y. T. Long, H. Tian, E. H. Sargent and Z. Ning, *Adv. Mater.*, 2017, **29**, 1605646.

19 T. F. Yeh, S. J. Chen and H. Teng, *Nano Energy*, 2015, **12**, 476-485.

20 Y. Li, K. Lv, W. Ho, F. Dong, X. Wu and Y. Xia, *Appl. Catal. B: Environ.*, 2017, **202**, 611-619.

21 R. Shen, J. Xie, Q. Xiang, X. Chen, J. Jiang and X. Li, *Chinese. J. Catal.*, 2019, **40**, 240-288.

22 Q. Tay, P. Kanhere, C. F. Ng, S. Chen, S. Chakraborty, A. C. H. Huan, T. C. Sum, R. Ahuja and Z. Chen, *Chem. Mater.*, 2015, **27**, 4930-4933.

23 S. Penner and M. Armbrüster, *ChemCatChem*, 2015, **7**, 374-392.

24 Y. Hou, Z. Wen, S. Cui, X. Guo and J. Chen, *Adv. Mater.*, 2013, **25**, 6291-6297.

25 B. Lin, G. Yang and L. Wang, *Angew. Chem. Int. Ed.*, 2019, **58**, 4587-4591.

26 S. S. Yi, J. M. Yan, B. R. Wulan, S. J. Li, K. H. Liu and Q. Jiang, *Appl. Catal. B: Environ.*, 2017, **200**, 477-483.

27 B. Lin, J. Li, B. Xu, X. Yan, B. Yang, J. Wei and G. Yang, *Appl. Catal. B: Environ.*, 2019, **243**, 94-105.

28 C. Li, Y. Du, D. Wang, S. Yin, W. Tu, Z. Chen, M. Kraft, G. Chen and R. Xu, *Adv. Funct. Mater.*, 2017, **27**, 1604328.

29 Y. Wang, X. Liu, J. Liu, B. Han, X. Hu, F. Yang, Z. Xu, Y. Li, S. Jia, Z. Li and Y. Zhao, *Angew. Chem. Int. Ed.*, 2018, **57**, 5765-5771.

30 Y. Zhang, L. Wu, X. Zhao, Y. Zhao, H. Tan, X. Zhao, Y. Ma, Z. Zhao, S. Song, Y. Wang and Y. Li, *Adv. Energy Mater.*, 2018, **8**, 1801139.

31 L. Zhang, N. Ding, L. Lou, K. Iwasaki, H. Wu, Y. Luo, D. Li, K. Nakata, A. Fujishima and Q. Meng, *Adv. Funct. Mater.*, 2018, **29**, 1806774.

32 H. Ou, L. Lin, Y. Zheng, P. Yang, Y. Fang and X. Wang, *Adv. Mater.*, 2017, **29**, 1700008.

33 Y. Xiao, G. Tian, W. Li, Y. Xie, B. Jiang, C. Tian, D. Zhao and H. Fu, *J. Am. Chem. Soc.*, 2019, **141**, 2508-2515.

34 J. Sun, J. Zhang, M. Zhang, M. Antonietti, X. Fu and X. Wang, *Nat. Commun.*, 2012, **3**, 1139.

35 W. Xing, W. Tu, Z. Han, Y. Hu, Q. Meng and G. Chen, *ACS Energy Lett.*, 2018, **3**, 514-519.

36 D. Ren, Z. Liang, Y. H. Ng, P. Zhang, Q. Xiang and X. Li, *Chem. Eng. J.*, 2020, **390**, 124496.

37 J. Di, C. Chen, S. Z. Yang, S. Chen, M. Duan, J. Xiong, C. Zhu, R. Long, W. Hao, Z. Chi, H. Chen, Y. X. Weng, J. Xia, L. Song, S. Li, H. Li and Z. Liu, *Nat. Commun.*, 2019, **10**, 2840.

38 C. Xue, P. Zhang, G. Shao and G. Yang, *Chem. Eng. J.*, 2020, **398**, 125602.

39 G. Zhang, G. Li, Z. A. Lan, L. Lin, A. Savateev, T. Heil, S. Zafeiratos, X. Wang and M. Antonietti, *Angew. Chem. Int. Ed.*, 2017, **56**, 13445-13449.

40 B. Lin, H. Li, H. An, W. Hao, J. Wei, Y. Dai, C. Ma and G. Yang, *Appl. Catal. B: Environ.*, 2018, **220**, 542-552.

41 J. Di, J. Xia, M. F. Chisholm, J. Zhong, C. Chen, X. Cao, F. Dong, Z. Chi, H. Chen, Y. X. Weng, J. Xiong, S. Z. Yang, H. Li, Z. Liu and S. Dai, *Adv. Mater.*, 2019, **31**, 1807576.

42 Y. Zhou, J. Zhang, E. Song, J. Lin, J. Zhou, K. Suenaga, W. Zhou, Z. Liu, J. Liu, J. Lou and H. J. Fan, *Nat. Commun.*, 2020, **11**, 2253.

43 J. Ran, W. Guo, H. Wang, B. Zhu, J. Yu and S. Z. Qiao, *Adv. Mater.*, 2018, **30**, 1800128.

44 Y. Zhou, Z. Zhou, R. Shen, R. Ma, Q. Liu, G. Cao and J. Wang, *Energy Storage Mater.*, 2018, **13**, 189-198.

45 D. Zeng, T. Zhou, W. J. Ong, M. Wu, X. Duan, W. Xu, Y. Chen, Y. A. Zhu and D. L. Peng, *ACS Appl. Mater. Interfaces*, 2019, **11**, 5651-5660.

46 H. Li, Y.Wu, C. Li, Y. Gong, L. Niu, X. Liu, Q. Jiang, C. Sun and S. Xu, *Appl. Catal. B: Environ.*, 2019, **251**, 305-312.

47 G. Zhao, Y. Sun, W. Zhou, X. Wang, K. Chang, G. Liu, H. Liu, T. Kako and J. Ye, *Adv. Mater.*, 2017, **29**, 1703258.

48 J. Di, J. Xiong, H. Li and Z. Liu, *Adv. Mater.*, 2018, **30**, 1704548.

49 B. Lin, A. Chaturvedi, J. Di, L. You, C. Lai, R. Duan, J. Zhou, B. Xu, Z. Chen, P. Song, J. Peng, B. Ma, H. Liu, P. Meng, G. Yang, H. Zhang, Z. Liu and F. Liu, *Nano Energy*, 2020, **76**, 104972.